Synthesis and Structural Characterization of Metallocrown Ethers Containing Butterfly Fe_2S_2 Cluster Cores. Biomimetic Hydrogen Evolution Catalyzed by $Fe_2(\mu\text{-}SCH_2CH_2OCH_2CH_2S\text{-}\mu)(CO)_6$

Li-Cheng Song,* Jie Gao, Hu-Ting Wang, Yu-Juan Hua, Hong-Tao Fan, Xiao-Guang Zhang, and Qing-Mei Hu

Department of Chemistry, State Key Laboratory of Elemento-Organic Chemistry, Nankai University, Tianjin 300071, People's Republic of China

Received August 6, 2006

The synthesis, structure, and properties of a series of new metallocrown ethers with butterfly Fe_2S_2 cluster cores have been investigated. While metallocrown ethers $Fe_2(\mu\text{-}SCH_2CH_2OCH_2CH_2S\text{-}\mu)(CO)_6$ (**I**) and $[Fe_2(\mu\text{-}SCH_2CH_2OCH_2CH_2S\text{-}\mu)(CO)_6]_2$ (**I***) were prepared in 30% yield by treatment of dithiol $HSCH_2CH_2OCH_2CH_2SH$ with equimolar $Fe_3(CO)_{12}$ in THF at 50−60 °C for 2 h, treatment of dithiols $HSCH_2(CH_2OCH_2)_nCH_2SH$ ($n = 2-4$) with equimolar $Fe_3(CO)_{12}$ in THF at reflux for 0.5 h afforded metallocrown ethers $Fe_2[\mu\text{-}SCH_2(CH_2OCH_2)_nCH_2S\text{-}\mu](CO)_6$ (**II**−**IV**) in 18−33% yields. In addition to a possible pathway for formation of these metallocrown ethers being suggested, all the metallocrown ethers have been fully characterized by elemental analysis and spectroscopy, as well as by X-ray crystallography for **I**, **III**, **IV**, and **I***. On the basis of electrochemical study of **I**−**IV**, metallocrown ether **I** was found to be a catalyst for proton reduction to hydrogen under electrochemical conditions. While an EECC mechanism for such catalytic H_2 evolution is suggested, the possibility for improving the catalytic activity of this crown ether by its complexation with a metal cations is predicted.

Introduction

Since crown ethers were discovered in 1967,[1] they have been receiving great attention because of their unique structures, valuable properties, and particularly important applications in various fields, such as supramolecular chemistry, catalysis, and material/life sciences.[2−6] Metallocrown ethers as a special class of crown ethers are of considerable interest, in which the mutual influence between their redox-active metal centers and the crown ether moiety or that complexed with metal cations could regulate and control their properties to give target compounds with the desired invaluable functions.[7,8] Previously, we reported some metallocrown ethers, such as those with redox-active tetrahedral M_2FeS (M = Mo or W) cluster cores[9] and the μ_4-S-containing Fe_4S_3 cluster cores.[10] Now, we wish to report the synthesis and structural characterization of a series of new metallocrown ethers, namely, $Fe_2[\mu\text{-}SCH_2(CH_2OCH_2)_nCH_2S\text{-}\mu](CO)_6$ ($n = 1-4$) and $[Fe_2(\mu\text{-}SCH_2CH_2OCH_2CH_2S\text{-}\mu)(CO)_6]_2$. In addition, the proton reduction to hydrogen catalyzed by the simplest member of this series is also described.

Results and Discussion

Synthesis and Spectroscopic Characterization of Metallocrown Ethers $Fe_2[\mu\text{-}SCH_2(CH_2OCH_2)_nCH_2S\text{-}\mu](CO)_6$ (I−IV) and $[Fe_2(\mu\text{-}SCH_2CH_2OCH_2CH_2S\text{-}\mu)(CO)_6]_2$ (I*). Metallocrown ethers **I**−**IV** and **I*** were prepared basically according to the well-known butterfly Fe_2S_2 cluster-forming reactions involving thiols with iron(0) carbonyl complexes.[11−14] Thus, treatment of a THF solution of $Fe_3(CO)_{12}$ with an equimolar amount of the ether chain-containing dithiol $HSCH_2CH_2OCH_2CH_2SH$ at 50−60 °C for 2 h afforded metallocrown ether **I** and its dimer **I*** in a total of 30% yield, whereas reaction of dithiols $HSCH_2(CH_2OCH_2)_nCH_2SH$ ($n = 2-4$) with $Fe_3(CO)_{12}$ in refluxing THF for 0.5 h resulted in formation of **II**−**IV** in 18−33% yields without the corresponding dimers being isolated (Scheme 1).

A possible pathway for formation of **I**−**IV** and **I*** is preliminarily suggested in Scheme 2. In the first step, the 16*e* species $Fe(CO)_4$ is formed in situ by decomposition of $Fe_3(CO)_{12}$. Then, addition of dithiols to $Fe(CO)_4$ gives the coordinatively saturated diiron intermediate $\mathbf{M_1}$. In the third step the coordinatively unsaturated diiron intermediate $\mathbf{M_2}$ is generated by elimination of H_2 and loss of its two CO ligands. Finally, the intramolecular cyclization of $\mathbf{M_2}$ ($n = 1-4$) produce **I**−**IV**, while the intermolecular dimerization of $\mathbf{M_2}$ ($n = 1$) affords dimer **I***.

* Corresponding author. Fax: 0086-22-23504853. E-mail: lcsong@nankai.edu.cn.

(1) Pederson, C. J. *J. Am. Chem. Soc.* **1967**, *89*, 7017.
(2) Gokel, G. W. *Crown Ethers and Cryptands, Monographs in Supramolecular Chemistry*; Royal Society of Chemistry: Cambridge, UK, 1991.
(3) Vögtle, F. *Supramolecular Chemistry, An Introduction*; Wiley: Chichester, UK, 1991.
(4) Lehn, J.-M. *Supramolecular Chemistry, Concepts and Perspectives*; VCH: Weinheim, 1995.
(5) Beer, P. D. *Adv. Inorg. Chem.* **1992**, *39*, 79.
(6) Van Veggel, F. C. J. M.; Verboom, W.; Reinhoudt, D. N. *Chem. Rev.* **1994**, *94*, 279.
(7) Plenio, H.; Burth, D. *Organometallics* **1996**, *15*, 1151.
(8) Saji, T. *Chem. Lett.* **1986**, 275.
(9) (a) Song, L.-C.; Guo, D.-S.; Hu, Q.-M.; Huang, X.-Y. *Organometallics* **2000**, *19*, 960. (b) Song, L.-C.; Guo, D.-S.; Hu, Q.-M.; Sun, J. *J. Organomet. Chem.* **2000**, *616*, 140. (c) Song, L.-C.; Guo, D.-S.; Hu, Q.-M.; Su, F.-H. Sun, J.; Huang, X.-Y. *J. Organomet. Chem.* **2001**, *622*, 210.
(10) (a) Song, L.-C.; Wang, J.-Y.; Gong, F.-H.; Cheng, J.; Hu, Q.-M. *J. Organomet. Chem.* **2004**, *689*, 930. (b) Song, L.-C.; Fan, H.-T.; Hu, Q.-M.; Yang, Z.-Y.; Sun, Y.; Gong F.-H. *Chem. Eur. J.* **2003**, *9*, 170.
(11) King, R. B. *J. Am. Chem. Soc.* **1963**, *85*, 1584.
(12) De Beer, J. A.; Haines, R. J. *J. Organomet. Chem.* **1970**, *24*, 757.
(13) Nametkin, N. S.; Tyurin, V. D.; Kukina, M. A. *J. Organomet. Chem.* **1978**, *149*, 355.
(14) Winter, A.; Zsolnai, L.; Huttner, G. *Z. Naturforsch.* **1982**, *37b*, 1430.

10.1021/om060711r CCC: $33.50
Publication on Web 10/18/2006

Scheme 1

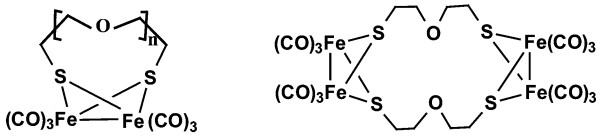

n	metallocrown ethers	
1	I	I*
2	II	
3	III	
4	IV	

Scheme 2

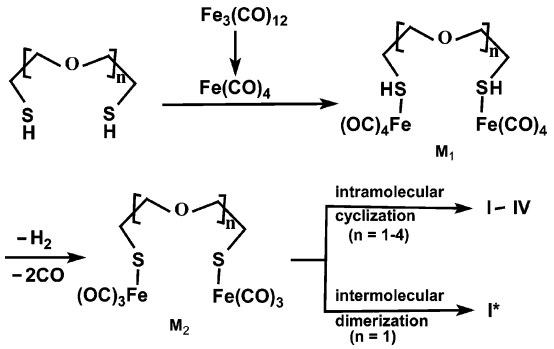

It should be noted that the pathway described in Scheme 2 seems to be plausible. This is because (i) a similar pathway was previously suggested for formation of the noncyclic analogues of **I**−**IV**, namely, $(\mu\text{-RS})_2Fe_2(CO)_6$, by reaction of RSH with $Fe_3(CO)_{12}$;[13] (ii) it was observed that some gases were evolved during reactions of $HSCH_2(CH_2OCH_2)_nCH_2SH$ (n = 1−4) with $Fe_3(CO)_{12}$; and particularly the evolved gases were identified as H_2 and CO by gas chromatographic analysis. However, at present, we are not very clear about the detailed pathway for formation of such metallocrown ethers, and thus more work remains to be done in the future.

Products **I**−**IV** and **I*** have been characterized by elemental analysis and spectroscopy. The IR spectra of **I**−**IV** and **I*** displayed four to five absorption bands in the range 2090−1959 cm^{-1} for their terminal carbonyls and one or two bands in the region 1141−1101 cm^{-1} for their ether chain functionality. The ^1H NMR spectrum of **I** showed one singlet at 2.54 ppm for protons in the two CH_2 groups attached to its two μ-S atoms, whereas **II**−**IV** each exhibited two singlets with an equal intensity in the range 2.63−2.29 ppm for the corresponding protons in CH_2 groups connected to their μ-S atoms, respectively. Consistent with their ^1H NMR spectra is that the ^{13}C NMR spectra of **I**−**IV** displayed one singlet at 33.72 ppm (for **I**) and two singlets at ca. 24 and 39 ppm (for **II**−**IV**) with an equal intensity for the carbon atoms in CH_2 groups attached to their μ-S atoms, respectively. This implies that the ether chain in **I** is only axially or equatorially bonded to the two μ-S atoms of the butterfly Fe_2S_2 cluster core, whereas that in each of **II**−**IV** is both axially and equatorially bonded to the two CH_2 groups of the corresponding butterfly Fe_2S_2 cluster core.[15,16] In fact, the ether chain in **I**, like the corresponding chain in biomimetic model $Fe_2(\mu\text{-SCH}_2)_2O(CO)_6$,[17] is only axially bonded to its two μ-S atoms in order to construct such a small crown ether (vide infra). Particularly noteworthy is that metallocrown ether **I*** contains two butterfly Fe_2S_2 cluster cores and it displayed two singlets at 2.27 and 2.72 ppm with an equal intensity in its ^1H NMR spectrum. Apparently, these two singlets can be assigned to the two pairs of terminal CH_2 groups in its two identical ether chains; the two ether chains are most likely connected to the μ-S atoms of the two butterfly Fe_2S_2 cluster cores by axial, equatorial, axial, and equatorial bonds, sequentially.[15,16] Fortunately, such a conformational assignment has been confirmed by its crystallographic study (vide infra).

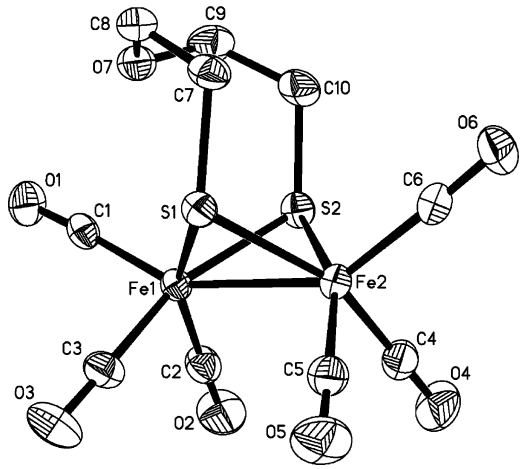

Figure 1. ORTEP drawing of **I** with 30% probability level ellipsoids.

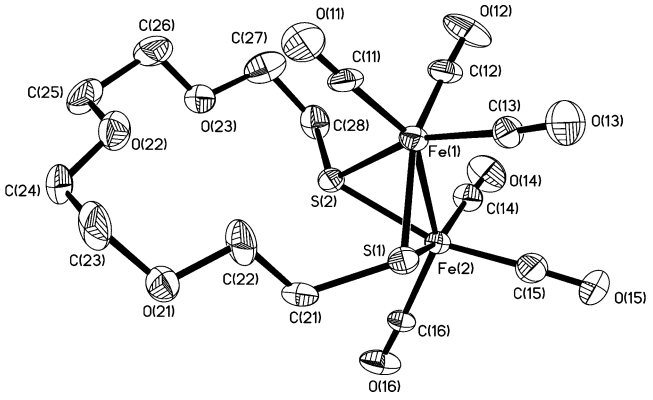

Figure 2. ORTEP drawing of **III** with 30% probability level ellipsoids.

Crystal Structures of Metallocrown Ethers I, III, IV, and I*. The molecular structures of **I**, **III**, **IV**, and **I*** have been unambiguously confirmed by X-ray diffraction analyses. Their ORTEP drawings are shown in Figures 1−4, whereas selected bond lengths and angles are given in Table 1. As can be seen in Figures 1−3, metallocrown ethers **I**, **III**, and **IV** each contain one butterfly Fe_2S_2 cluster core that carries a pair of three terminal carbonyls at its Fe atoms and is linked via its S atoms with an ether chain. In addition, it is clearly seen that the ether chain of **I** is indeed axially bonded to the two μ-S atoms ($\angle$C7−S1···S2 = $\angle$C10−S2···S1 = 89.1°), whereas that of **III** or **IV** is connected to the two μ-S atoms by an axial ($\angle$C21−S1···S2 = 78.1°, $\angle$C7−S1···S2 = 79.5°) and an equatorial ($\angle$C28−S2···S1 = 163.0°, $\angle$C16−S2···S1 = 159.0°) type of bond, respectively. Figure 4 shows that metallocrown ether **I*** is a dimer of **I** in which one ether chain is axially and equatorially bonded to S1/S2 atoms ($\angle$C13−S1···S3 = 80.3°, $\angle$C16−S2···S4 = 160.6°) and the other chain is axially and equatorially bonded to S4/S3 atoms ($\angle$C17−S4···S2 = 77.6°, $\angle$C20−S3···S1 = 158.3°), respectively.

(15) Shaver, A.; Fitzpatrick, P. J.; Steliou, K.; Butler, I. S. *J. Am. Chem. Soc.* **1979**, *101*, 1313.

(16) Seyferth, D.; Henderson, R. S.; Song, L.-C. *Organometallics* **1982**, *1*, 125.

(17) Song, L.-C.; Yang, Z.-Y.; Bian, H.-Z; Liu, Y.; Wang, H.-T.; Liu, X.-F.; Hu, Q.-M. *Organometallics* **2005**, *24*, 6126.

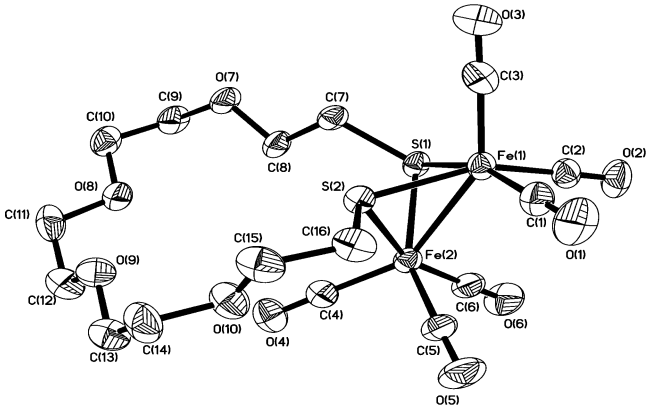

Figure 3. ORTEP drawing of **IV** with 30% probability level ellipsoids.

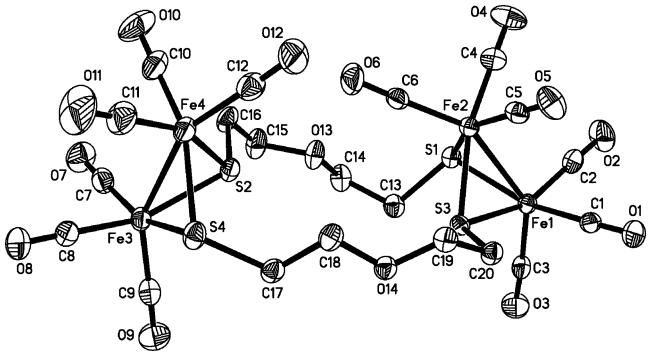

Figure 4. ORTEP drawing of **I*** with 30% probability level ellipsoids.

Finally, it is worth pointing out that the geometric parameters related to the butterfly Fe_2S_2 cluster cores in these metallocrown ethers are very close to the corresponding parameters reported for other butterfly Fe_2S_2 cluster complexes. For example, the Fe−Fe bond lengths and the Fe−S−Fe bond angles of **I**, **III**, **IV**, and **I*** are respectively 2.5064−2.5277 Å and 66.80−68.24°, whereas the corresponding bonds and angles of $(\mu\text{-EtS})_2Fe_2(CO)_6$[18] and $Fe_2(\mu\text{-SCH}_2)_2O(CO)_6$[17] are 2.5113−2.537 Å and 67.76−68.88°, respectively.

Electrochemistry of Metallocrown Ethers I−IV. In view of the structural similarity of metallocrown ethers **I**−**IV** with biomimetic model $Fe_2(\mu\text{-SCH}_2)_2O(CO)_6$,[17] we decided to examine their electrochemical properties and to see if **I** could have the electrocatalytic activity for proton reduction to hydrogen. The electrochemical behavior of **I**−**IV** was investigated by cyclic voltammetry in MeCN under N_2. Table 2 lists their electrochemical data, while Figure 5 as a representative shows the cyclic voltammogram of **1**. It is shown that metallocrown ethers **I**−**IV** each display one quasi-reversible reduction process, one irreversible reduction process, and one irreversible oxidation process. The first reduction process ($E_{pc} = -1.51$ to -1.66 V) is a one-electron process (supported by bulk electrolysis), which can be assigned to the reduction of Fe^IFe^I to Fe^IFe^0. Similarly, the second reduction process ($E_{pc} = -2.28$ to -2.31 V) or the oxidation process ($E_{pa} = +0.54$ to $+0.64$ V) is also a one-electron process; they can be ascribed to the reduction of Fe^IFe^0 to Fe^0Fe^0 and the oxidation of Fe^IFe^I to Fe^IFe^{II}, respectively. It follows that the electrochemical properties of **I**−**IV** described above are very similar to those displayed by biomimetic model $Fe_2(\mu\text{-SCH}_2)_2O(CO)_6$.[17]

The electrocatalytic activity of **I** was found by measuring the cyclic voltammograms of **I** with HOAc (0−10 mM) in MeCN under N_2 (Figure 6). As shown in Figure 6, when 2 mM HOAc was added to the MeCN solution of **I** without HOAc, its cyclic voltammogram displayed a new peak at $E_{pc} = -1.61$ V compared to that of **I** without HOAc, but it disappeared when this HOAc-containing MeCN solution was saturated with CO. So, this new peak was supposed to be generated by reduction of the species $HFe^{II}-Fe^I$ (formed by oxidative addition of a proton to the prereduced Fe^IFe^0 followed by CO substitution with MeCN).[19] In addition, as can be seen in the cyclic voltammograms with HOAc (2−10 mM), the original first peak at $E_{pc} = -1.51$ V in the cyclic voltammogram of **I** without HOAc was just slightly increased (the new peak at $E_{pc} = -1.61$ V was also slightly increased), but the original second peak at $E_{pc} = -2.28$ V in that of **I** without HOAc grew

Table 1. Selected Bond Lengths (Å) and Angles (deg) for I, III, IV, and I*

I			
Fe(1)−S(1)	2.2708(10)	Fe(2)−S(2)	2.2723(9)
Fe(1)−S(2)	2.2658(10)	O(7)−C(9)	1.406(4)
O(7)−C(8)	1.396(4)	Fe(1)−Fe(2)	2.5064(8)
Fe(2)−S(1)	2.2655(10)	S(1)−C(7)	1.830(3)
S(1)−Fe(2)−Fe(1)	56.56(2)	Fe(2)−S(1)−Fe(1)	67.08(3)
S(2)−Fe(2)−S(1)	87.91(3)	C(7)−S(1)−Fe(1)	120.49(10)
S(2)−Fe(2)−Fe(1)	56.35(3)	C(8)−O(7)−C(9)	116.8(3)
S(1)−Fe(1)−S(2)	87.95(3)	Fe(1)−S(2)−Fe(2)	67.05(3)
S(1)−Fe(1)−Fe(2)	56.36(3)	Fe(2)−Fe(1)−S(2)	56.60(2)
III			
Fe(1)−S(1)	2.253(3)	O(21)−C(22)	1.447(13)
Fe(1)−S(2)	2.243(3)	O(22)−C(24)	1.346(16)
Fe(2)−S(2)	2.254(3)	Fe(1)−Fe(2)	2.517(2)
Fe(2)−S(1)	2.265(4)	O(23)−C(26)	1.326(14)
S(2)−Fe(1)−Fe(2)	56.19(8)	Fe(2)−S(1)−Fe(1)	67.69(10)
S(1)−Fe(1)−Fe(2)	56.38(10)	Fe(1)−S(2)−Fe(2)	68.06(9)
S(2)−Fe(2)−S(1)	79.40(11)	C(22)−O(21)−C(23)	104.8(10)
S(2)−Fe(2)−Fe(1)	55.75(8)	C(24)−O(22)−C(25)	112.0(9)
S(1)−Fe(2)−Fe(1)	55.93(9)	C(26)−O(23)−C(27)	111.4(10)
IV			
Fe(1)−S(1)	2.2679(17)	O(7)−C(8)	1.399(6)
Fe(1)−S(2)	2.2523(16)	C(10)−O(8)	1.412(6)
Fe(2)−S(2)	2.2511(16)	Fe(1)−Fe(2)	2.5234(12)
Fe(2)−S(1)	2.2641(16)	C(12)−O(9)	1.392(7)
S(1)−Fe(1)−Fe(2)	56.09(4)	S(1)−Fe(2)−Fe(1)	56.24(4)
S(2)−Fe(1)−S(1)	80.74(5)	Fe(2)−S(1)−Fe(1)	67.67(4)
S(2)−Fe(1)−Fe(2)	55.90(4)	Fe(2)−S(2)−Fe(1)	68.16(5)
S(2)−Fe(2)−S(1)	80.85(6)	C(8)−O(7)−C(9)	113.6(4)
S(2)−Fe(2)−Fe(1)	55.95(5)	C(10)−O(8)−C(11)	113.1(5)
I*			
Fe(1)−S(1)	2.2685(16)	Fe(2)−S(3)	2.2485(15)
Fe(1)−S(3)	2.2575(15)	O(14)−C(19)	1.421(6)
O(13)−C(14)	1.410(6)	Fe(1)−Fe(2)	2.5276(12)
Fe(2)−S(1)	2.2672(15)	S(1)−C(13)	1.824(5)
S(3)−Fe(1)−S(1)	80.89(5)	S(1)−Fe(2)−Fe(1)	56.16(4)
S(3)−Fe(1)−Fe(2)	55.71(4)	C(13)−S(1)−Fe(1)	109.28(19)
S(1)−Fe(1)−Fe(2)	56.11(4)	C(16)−S(2)−Fe(3)	117.55(19)
S(3)−Fe(2)−S(1)	81.12(5)	C(18)−O(14)−C(19)	113.3(4)
S(3)−Fe(2)−Fe(1)	56.05(4)	C(14)−O(13)−C(15)	111.6(4)

Table 2. Electrochemical Data of I-IV[a]

compound	E_{pc}, E_{pa}[V] Fe^IFe^I/Fe^IFe^0	E_{pc}[V] Fe^IFe^0/Fe^0Fe^0	E_{pa}[V] Fe^IFe^I/Fe^IFe^{II}
I	−1.51, −1.38	−2.28	+0.54
II	−1.63, −1.50	−2.24	+0.58
III	−1.64, −1.44	−2.30	+0.59
IV	−1.66, −1.47	−2.31	+0.64

[a] All potentials are versus Fc/Fc^+ in 0.1 M $n\text{-}Bu_4NPF_6$/MeCN.

(18) Dahl, L. F.; Wei, C.-H. *Inorg. Chem.* **1963**, *2*, 328.

(19) Chong, D.; Georgakaki, I. P.; Mejia-Rodriguez, R.; Sanabria-Chinchilla, J.; Soriaga, M. P.; Darensbourg, M. Y. *Dalton Trans.* **2003**, *3*, 4158.

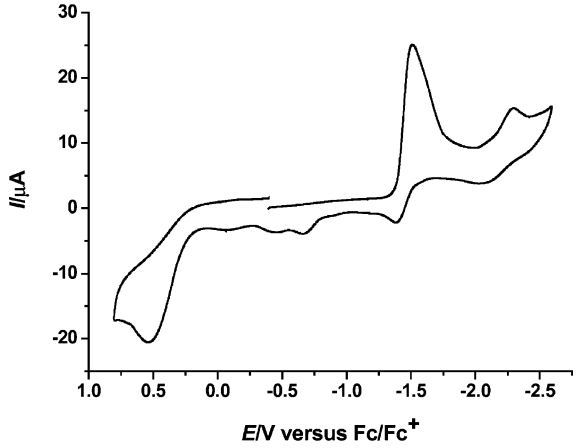

Figure 5. Cyclic voltammogram of **I** (1.0 mM) in 0.1 M *n*-Bu_4NPF_6/MeCN at a scan rate of 100 mV × s^{-1}.

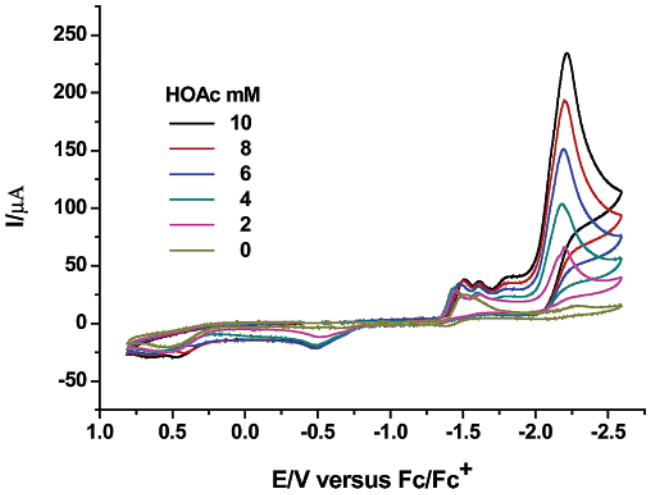

Figure 6. Cyclic voltammograms of **I** (1.0 mM) with HOAc (0−10 mM) at a scan rate of 100 mV × s^{-1}.

up linearly with sequential increments of HOAc. Such observations feature an electrochemical catalytic process.[19−24]

The electrocatalytic process was further confirmed by bulk electrolysis of a MeCN solution of **I** (0.50 mM) with HOAc (25 mM) at −2.30 V. A total of 11.2 F per mol of **I** passed during half an hour, which corresponds to 5.6 turnovers. Gas chromatographic analysis showed that the hydrogen yield was nearly 100%.

Scheme 3 illustrates an EECC mechanism (E = electrochemical, C = chemical) suggested for this electrocatalytic H_2 evolution based on the reported similar cases[19−24] and the above-mentioned electrochemical observations. In the presence of HOAc, the $[Fe^I-Fe^I]$ metallocrown ether **I** will first undergo one-electron reduction at −1.51 V to form the $[Fe^I-Fe^0]^-$ monoanion $\mathbf{I}^-$. Further reduction of $\mathbf{I}^-$ at −2.28 V affords the $[Fe^0-Fe^0]^{2-}$ dianion $\mathbf{I}^{2-}$, which is then protonated on one of

Scheme 3

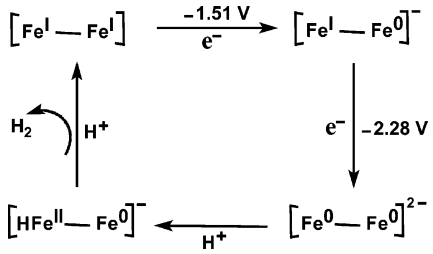

its electron-rich Fe atoms by HOAc to produce the $[HFe^{II}-Fe^0]^-$ monoanion $\mathbf{IH}^-$. Finally, further protonation of $\mathbf{IH}^-$ results in formation of hydrogen to complete the catalytic cycle.

In summary, we have synthesized the five new metallocrown ethers **I**−**IV** and **I*** by thermal reactions of dithiols $HSCH_2(CH_2OCH_2)_nCH_2SH$ (n = 1−4) with $Fe_3(CO)_{12}$ under appropriate conditions. On the basis of structural characterization of all the metallocrown ethers and the electrochemical study of **I**−**IV**, metallocrown ether **I** has been proved, like biomimetic model $Fe_2(\mu\text{-}SCH_2)_2O(CO)_6$,[17] to be a catalyst for reducing proton to hydrogen under electrochemical conditions. In view of the well-known coordination ability of crown ethers with various metal cations,[2−4] it can be expected that the catalytic activity of metallocrown ether **I** could be improved by complexation of its O/S heteroatoms with suitable metal cations. This is because the complexed metal cations such as Na^+ and K^+ would be able to decrease the reduction potential of the catalytic centers of Fe atoms and thus make proton reduction occur more easily. Further studies on metallocrown ether **I** as well as the others reported here are in progress along this direction.

Experimental Section

General Comments. All reactions were carried out under an atmosphere of prepurified nitrogen using standard Schlenk and vacuum-line techniques. Tetrahydrofuran (THF) was distilled from Na/benzophenone ketyl under nitrogen. $HSCH_2(CH_2OCH_2)_nCH_2SH$ (n = 1−4)[25] and $Fe_3(CO)_{12}$[26] were prepared according to literature procedures. Preparative TLC was carried out on glass plates (26 × 20 × 0.25 cm) coated with silica gel H (10−40 μm). IR spectra were recorded on a Nicolet Magna 560 FTIR or a Bruker Vector 22 infrared spectrophotometer. ^1H NMR spectra were obtained on a Bruker AC-P200 or a Bruker Avance 300 NMR spectrometer, while ^{13}C NMR spectra were obtained on a Varian Mercury Plus 400 NMR spectrometer. C/H analyses were performed on an Elementar Vario EL analyzer. Melting points were determined on a Yanaco MP-500 apparatus and were uncorrected.

Preparation of $Fe_2[\mu\text{-}SCH_2CH_2OCH_2CH_2S\text{-}\mu](CO)_6$ (I) and $[Fe_2(\mu\text{-}SCH_2CH_2OCH_2CH_2S\text{-}\mu)(CO)_6]_2$ (I*). A 100 mL three-necked flask equipped with a stir-bar, a serum cap, and a nitrogen inlet tube was charged with 1.00 g (1.98 mmol) of $Fe_3(CO)_{12}$, 0.24 mL (2.00 mmol) of $HSCH_2CH_2OCH_2CH_2SH$, and 30 mL of THF. The green solution was stirred at 50−60 °C for 2 h, resulting in a color change from green to red. Solvent was removed in vacuo, and the residue was subjected to TLC using CH_2Cl_2/petroleum ether (1:2 v/v) as eluent. From the first red band 0.153 g (19%) of **I** was obtained as a red solid, mp 45 °C dec Anal. Calcd for $C_{10}H_8Fe_2O_7S_2$: C, 28.87; H, 1.94. Found: C, 28.85; H, 1.96. IR (KBr disk): $\nu_{C\equiv O}$ 2069(s), 2023(vs), 1992(vs), 1977(s), 1965(vs); ν_{C-O-C} 1101(m) cm^{-1}. ^1H NMR ($CDCl_3$): 2.54 (s, 4H, 2 a-SCH_2), 3.57(s, 4H, $2CH_2O$) ppm. $^{13}C\{^1H\}$ NMR (100.6 MHz, $CDCl_3$): 207.65

(20) Bhugun, I.; Lexa, D.; Saveant, J.-M. *J. Am. Chem. Soc.* **1996**, *118*, 3982.
(21) Gloaguen, F.; Lawrence, J. D.; Rauchfuss, T. B. *J. Am. Chem. Soc.* **2001**, *123*, 9476.
(22) Ott, S.; Kritikos, M.; Åkermark, B.; Sun, L.; Lomoth, R. *Angew. Chem., Int. Ed.* **2004**, *43*, 1006.
(23) Borg, S. J.; Behrsing, T.; Best, S. P.; Razavet, M.; Liu, X.; Pickett, C. J. *J. Am. Chem. Soc.* **2004**, *126*, 16988.
(24) Capon, J.-F.; Gloaguen, F.; Schollhammer, P.; Talarmin, J. *Coord. Chem. Rev.* **2005**, *249*, 1664.
(25) Speziale, A. J. *Organic Syntheses*; J. Wiley & Sons, Inc.: New York, 1963; Collect. Vol. 4, p 401.
(26) King, R. B. *Organometallic Syntheses; Transition-Metal Compounds*; Academic Press: New York, 1965; Vol. 1, p 95.

Table 3. Crystal Data and Structural Refinement Details for I, III, IV, and I*

	I	III	IV	I*
mol formula	$C_{10}H_8Fe_2O_7S_2$	$C_{28}H_{32}Fe_4O_{18}S_4$	$C_{32}H_{40}Fe_4O_{20}S_4$	$C_{20}H_{16}Fe_4O_{14}S_4$
mol wt	415.98	1008.18	1096.28	831.97
cryst syst	monoclinic	triclinic	monoclinic	monoclinic
space group	$P2(1)/n$	$P\bar{1}$	$C2/c$	$P2(1)/c$
a/Å	7.771 (2)	11.3991(10)	24.931(10)	15.933(5)
b/Å	16.806(5)	14.2960(16)	8.330(3)	10.426(3)
c/Å	11.910(4)	14.8001(11)	22.685(9)	38.005(11)
α/deg	90	68.1460(10)	90	90
β/deg	103.515(5)	68.9940(10)	94.437(13)	95.643(5)
γ/deg	90	88.697(2)	90	90
V/Å^3	1512.4(8)	2072.6(3)	4697(3)	6282(3)
Z	4	4	4	8
D_c/g·cm^{-3}	1.827	3.231	1.550	1.759
abs coeff/mm^{-1}	2.219	3.284	1.459	2.137
F(000)	832	2048	2240	3328
$2\theta_{max}$/deg	50.02	52.82	50.06	52.86
no. of reflns	7719	11 317	9436	33 557
no. of indep reflns	2668	9841	4144	12 808
index ranges	$-4 \le h \le 9$	$-13 \le h \le 14$	$-29 \le h \le 20$	$-16 \le h \le 19$
	$-19 \le k \le 19$	$-9 \le k \le 17$	$-9 \le k \le 9$	$-13 \le k \le 11$
	$-14 \le l \le 13$	$-13 \le l \le 18$	$-27 \le l \le 26$	$-47 \le l \le 47$
goodness of fit	1.027	1.020	0.953	1.027
R	0.0295	0.0320	0.0405	0.0566
R_w	0.0571	0.0816	0.0817	0.0945
largest diff peak and hole/e Å^{-3}	0.365/−0.250	0.409/−0.275	0.296/−0.298	0.494/−0.378

(s, 6C, 6CO), 67.05 (s, 2C, 2CH_2O), 33.72 (s, 2C, 2 a-SCH_2) ppm. From the second red band 0.088 g (11%) of **I*** was obtained as a red solid, mp 128−129 °C. Anal. Calcd for $C_{20}H_{16}Fe_4O_{14}S_4$: C, 28.87; H, 1.94. Found: C, 28.79; H, 1.90. IR (KBr disk): $\nu_{C\equiv O}$ 2072(s), 2039(vs), 1995(vs), 1979(vs); ν_{C-O-C} 1118(s), 1093(m) cm^{-1}. ^{1}H NMR ($CDCl_3$): 2.27 (s, 4H, 2 a-SCH_2), 2.72 (s, 4H, 2 e-SCH_2), 3.34, 3.78 (2s, 8H, 4CH_2O) ppm.

Preparation of $Fe_2[\mu$-$SCH_2(CH_2OCH_2)_2CH_2S$-$\mu](CO)_6$ (II). A 100 mL three-necked flask fitted with a stir-bar, a serum cap, and a reflux condenser topped with a nitrogen inlet tube was charged with 1.00 g (1.98 mmol) of $Fe_3(CO)_{12}$, 0.32 mL (2.00 mmol) of $HSCH_2(CH_2OCH_2)_2CH_2SH$, and 30 mL of THF. After the green mixture was stirred at reflux for 0.5 h, solvent was removed in vacuo and the residue was subjected to TLC using CH_2Cl_2 as eluent. From the main red band 0.160 g (17%) of **II** was obtained as a red solid, mp 150 °C dec. Anal. Calcd for $C_{12}H_{12}Fe_2O_8S_2$: C, 31.33; H, 2.63. Found: C, 31.44; H, 2.60. IR (KBr disk): $\nu_{C\equiv O}$ 2090(s), 2034(vs), 1993(vs), 1966(vs); ν_{C-O-C} 1137(m), 1113(m) cm^{-1}. ^{1}H NMR ($CDCl_3$): 2.29 (s, 2H, a-SCH_2), 2.61 (s, 2H, e-SCH_2), 3.50−3.80 (m, 8H, 4CH_2O) ppm. $^{13}C\{^1H\}$ NMR (100.6 MHz, $CDCl_3$): 208.82 (s, 6C, 6CO), 71.61 (s, 2C, 2CH_2O), 71.34, 70.49 (2s, 2C, 2CH_2O), 39.48 (s, 1C, e-SCH_2), 24.92 (s, 1C, a-SCH_2) ppm.

Preparation of $Fe_2[\mu$-$SCH_2(CH_2OCH_2)_3CH_2S$-$\mu](CO)_6$ (III). The same equipped flask and procedure was utilized as for **II**, except that 0.40 mL (2.00 mmol) of $HSCH_2(CH_2OCH_2)_3CH_2SH$ was used instead of $HSCH_2(CH_2OCH_2)_2CH_2SH$. From the main red band 0.210 g (21%) of **III** was obtained as a red solid, mp 92−93 °C. Anal. Calcd for $C_{14}H_{16}Fe_2O_9S_2$: C, 33.36; H, 3.20. Found: C, 33.76; H, 3.26. IR (KBr disk): $\nu_{C\equiv O}$ 2069(s), 2032(vs), 1992(vs), 1974(s), 1959(s); ν_{C-O-C} 1127(m), 1098(m) cm^{-1}. ^{1}H NMR ($CDCl_3$): 2.40 (s, 2H, a-SCH_2), 2.63 (s, 2H, e-SCH_2), 3.30−3.95 (m, 12H, 6CH_2O) ppm. $^{13}C\{^1H\}$ NMR (100.6 MHz, $CDCl_3$): 209.01 (s, 6C, 6CO), 72.53, 71.23, 70.89, 70.72, 69.85, 69.80 (6s, 6C, 6CH_2O), 38.60 (s, 1C, e-SCH_2), 22.91 (s, 1C, a-SCH_2) ppm.

Preparation of $Fe_2[\mu$-$SCH_2(CH_2OCH_2)_4CH_2S$-$\mu](CO)_6$ (IV). The same equipped flask and procedure were employed as for **II**, except that 0.50 mL (2.00 mmol) of $HSCH_2(CH_2OCH_2)_4CH_2SH$ was used instead of $HSCH_2(CH_2OCH_2)_2CH_2SH$, using petroleum ether/acetone (2:1 v/v) as eluent. From the main red band 0.360 g (33%) of **IV** was obtained as a red solid, mp 70−72 °C. Anal. Calcd for $C_{16}H_{20}Fe_2O_{10}S_2$: C, 35.06; H, 3.68. Found: C, 35.00; H, 3.50. IR (KBr disk): $\nu_{C\equiv O}$ 2074(vs), 2034(vs), 1997(vs), 1962(vs); ν_{C-O-C} 1141(m), 1109(s) cm^{-1}. ^{1}H NMR ($CDCl_3$): 2.37 (s, 2H, a-SCH_2), 2.63 (s, 2H, e-SCH_2), 3.40−3.82 (m, 16H, 8CH_2O) ppm. $^{13}C\{^1H\}$ NMR (100.6 MHz, $CDCl_3$): 208.88 (s, 6C, 6CO), 72.09, 71.43, 71.17, 71.08, 70.95, 70.90, 70.61, 70.50 (8s, 8C, 8CH_2O), 39.29 (s, 1C, e-SCH_2), 23.25 (s, 1C, a-SCH_2) ppm.

X-ray Structure Determinations of I, III, IV, and I*. Single crystals of **I**, **III**, **IV**, and **I*** suitable for X-ray diffraction analyses were grown by slow evaporation of the CH_2Cl_2/hexane solutions of **I** and **I*** or the Et_2O/petroleum ether solutions of **III** and **IV** at about 4 °C. Each crystal was mounted on a Bruker SMART 1000 automated diffractometer. Data were collected at room temperature, using a graphite monochromator with Mo Kα radiation (λ = 0.71073 Å) in the $\omega-\phi$ scanning mode. Absorption correction was performed using the SADABS program.[27] The structures were solved by direct methods using the SHELXS-97 program[28] and refined by full-matrix least-squares techniques (SHELXL-97)[29] on F^2. Hydrogen atoms were located by using the geometric method. Details of crystal data, data collections, and structure refinements are summarized in Table 3.

Electrochemistry. Acetonitrile (Fisher Chemicals, HPLC grade) was used for electrochemistry assays. A solution of 0.1 M n-Bu_4NPF_6 in MeCN was used as electrolyte in all cyclic voltammetric experiments. The electrolyte solution was degassed by bubbling with N_2 or CO for 10 min before measurement. Electrochemical measurements were made using a BAS Epsilon potentiostat. All voltammograms were obtained in a three-electrode cell with a 3 mm diameter glassy carbon working electrode, a platinum counter electrode, and an Ag/Ag^+ (0.01 M $AgNO_3$/0.1 M n-Bu_4NPF_6 in MeCN) reference electrode under nitrogen atmosphere. The working electrode was polished with 0.05 μm alumina paste and sonicated in water for 10 min prior to use. Bulk electrolysis was run on a vitreous carbon rod (ca. 3 cm^2) in a two-compartment, gastight, H-type electrolysis cell containing ca. 20 mL of MeCN. Voltammograms were corrected for the effects of iR drop using a positive feedback approach implemented within the epsilon software. All potentials are quoted against the ferrocene/ferrocenium (Fc/Fc^+) potential. Gas chromatography was performed with a Shimadzu

(27) Sheldrick, G. M. *SADABS, A Program for Empirical Absorption Correction of Area Detector Data*; University of Göttingen: Germany, 1996.
(28) Sheldrick, G. M. *SHELXS97, A Program for Crystal Structure Solution*; University of Göttingen: Germany, 1997.
(29) Sheldrick, G. M. *SHELXL97, A Program for Crystal Structure Refinement*; University of Göttingen: Germany, 1997.

gas chromatograph GC-9A under isothermal conditions with nitrogen as a carrier gas and a thermal conductivity detector.

Acknowledgment. We are grateful to the National Natural Science Foundation of China and the Specialized Research Fund for the Doctoral Program of Higher Education of China for financial support of this work.

Supporting Information Available: Full tables of crystal data, atomic coordinates and thermal parameters, and bond lengths and angles for **I**, **III**, **IV**, and **I*** as CIF files. This material is available free of charge via the Internet at http://pubs.acs.org.

OM060711R